Hindawi
Advances in Meteorology
Volume 2019, Article ID 3428786, 9 pages
https://doi.org/10.1155/2019/3428786

Research Article

Use of the C-Band Microwave Link to Distinguish between Rainy and Dry Periods

Binsheng He, Xichuan Liu, Shuai Hu, Kun Song, and Taichang Gao

College of Meteorology and Oceanography, National University of Defense Technology, Nanjing 211101, China

Correspondence should be addressed to Xichuan Liu; liuxc85@gmail.com

Received 1 April 2019; Revised 3 July 2019; Accepted 10 July 2019; Published 21 July 2019

Academic Editor: Stefania Bonafoni

As a method that does not require additional cost, precipitation measurement by microwave links (MLs) has quickly attracted the attention of experts in meteorological, hydrological, and other related fields, of which wet-dry classification by MLs is one of the most important methods. Considering that existing commercial MLs are usually single-path, single-polarization, or low-frequency MLs, this paper uses the C-band ML and analyzes the variation in the receive signal level (RSL) of the C-band ML under the conditions of no rain, drizzle, light rain, and moderate rain. The RSL data are analyzed at different time scales by using long short-term memory (LSTM) network techniques, and then the method for distinguishing parts of the precipitation period by using the RSL from low-frequency MLs is proposed and validated. The results show that wet-dry classification is ideal. The accuracy on each day was higher than 60%, and some days had accuracies that were even higher than 98%. MLs below 10 GHz also had the potential to monitor ground rainfall. This study will broaden the range of available equipment for MLs for precipitation measurement.

1. Introduction

The accurate measurement of the intensity and spatial distribution of precipitation is of great significance for meteorology-related fields. In areas with complex terrain and uneven precipitation distribution, the influences of the spatial and temporal distributions of precipitation on mountain flood warnings and urban flood forecasting cannot be ignored. For mountains, cities, and forest areas, weather stations are sparsely distributed, and there may be a lack of dedicated rain measurement equipment. In 2006, Messer et al. [1] proposed the use of widely distributed commercial microwave links (MLs) for precipitation measurement. The signal is attenuated by the precipitation particles along the propagation path, and the attenuation caused by precipitation has a power-law relationship with rain intensity. Rain-induced attenuation in commercial MLs can be used to inverse the precipitation information, which can lead to the development of a novel approach for precipitation measurement. As a method that does not require additional cost, precipitation measurement by MLs has quickly attracted the attention of experts in related fields. In recent years, the rain measurement technology using MLs has become more sophisticated, and many scholars from various countries have made remarkable progress [2–5].

Among the technical aspects of measuring precipitation using MLs, the wet-dry classification is one of the most important core technologies [6]. The wet-dry classification is usually used to identify the precipitation period based on the receive signal level (RSL) from the MLs. The attenuation of MLs can be categorized into two types: precipitation-induced attenuation (caused by raindrops, snowflakes, and other precipitation particles) and nonprecipitation-induced attenuation (caused by path fading, water vapor, and gas absorption). Nonprecipitation-induced attenuation is also called base attenuation when measuring precipitation by MLs; if the nonprecipitation-induced attenuation is mistakenly considered precipitation-induced attenuation, the rainfall intensity inversed by the attenuation of MLs tends to be overestimated. Therefore, it is first necessary to eliminate the interference of nonprecipitation-induced attenuation and accurately extract precipitation-induced attenuation from MLs.

By using the differences in the RSL before and after precipitation to estimate the base attenuation of the precipitation period, attenuation during precipitation caused by other factors can be largely eliminated. Therefore, the wet-dry classification is closely related to the calculation of base attenuation. These two types of problems are collectively referred to as baseline estimation problems [7]. Based on the complex time distribution of the ML RSL, relevant scholars have carried out a series of studies on the baseline estimation problems. Leijnse et al. [8] summarized the signal characteristics of the precipitation period based on a large amount of data and set a threshold for the differentiation between wet and dry periods. To reduce the interference caused by complex uncertainties, Goldshtein et al. [9] used single-path multiband MLs to calculate accurate precipitation periods. Ruf et al. [10] used dual-polarized MLs to compare the signal characteristics of different levels of polarization to eliminate interference from nonprecipitation factors. Harel and Messer [11] used the likelihood ratio test to estimate the unknown parameters of the signal level to determine rain-induced attenuation.

However, the above research is all based on MLs with frequencies higher than 10 GHz, where rain-induced attenuation is higher. In fact, MLs with single-path, single-polarization, and low-frequency features occupy a very high proportion of the communication networks. For the lower frequency MLs, the precipitation-induced attenuation is lower than the attenuation at higher frequencies; therefore, the uncertainty in the signal transmission power, nonstationary noise, and other unstable factors will cause more errors in the precipitation measurements, especially for light rainfall. Therefore, it is more difficult to inverse the precipitation using low-frequency MLs. To promote the application of MLs with lower frequencies in precipitation measurements, this paper explores the C-band ML to distinguish rainy from dry periods.

In this paper, signal data are analyzed at various time scales and combined with the long short-term memory (LSTM) network. The experimental data are introduced in Section 2. The classification strategy based on the RSL characteristics and the LSTM network model are discussed in Section 3. The results are discussed in Section 4. Finally, the conclusions are given in Section 5.

2. Experimental Data

The experimental data were collected from commercial microwave equipment belonging to the Jiangsu Maritime Administration of China. The frequency of the ML was 7.7 GHz. The transmitting and receiving terminals were located at Yizheng (32.2522°N, 119.1410°E) and Qixia Mountain (32.1590°N, 118.9625°E), Nanjing, China. The length of the ML was 19.74 km. The data were the RSL at the receiving terminal, with a resolution of 0.1 dB, which can be recorded 11 times per minute; therefore, the temporal resolution was approximately 5.45 seconds. A tipping bucket rain gauge was located at the receiving terminal at Qixia Mountain to record the precipitation intensity.

The experiment was conducted from 1 November to 31 December 2018. No data were collected from 13 to 21 December 2018 because of equipment maintenance; therefore, 55 days of experimental data were collected. According to the results recorded by the rain gauge, except for rainfall on 3rd December reaching a rain rate of 36 mm/h, most of the precipitation was light rain, with a rain rate ≤12 mm/h. The geographical distribution of the MLs and the experimental equipment are shown in Figure 1.

According to the original RSL data from the MLs under clear-sky conditions, the RSL showed complex temporal characteristics: three unique characteristics in total (Figure 2). First, there was a sudden interval change in the RSL, and the duration of the signal variation was less than 2 min. Second, the relevant parameters of the RSL changed over time. Third, the frequency and amplitude of noise had random variations over time.

3. Methods

3.1. Classification Strategy Based on Signal Attenuation Characteristics. The attenuation of the ML can be expressed as

$$A(t) = \begin{cases} A_B(t), & \text{if dry,} \\ A_B(t) + A_R(t), & \text{if rain,} \end{cases} \quad (1)$$

where $A(t)$ is the total attenuation (dB) of the ML, A_B (dB) is the attenuation caused by nonprecipitation factors, and A_R is the rain-induced attenuation. For the MLs with stable power and high frequency, the A_R is very significant when precipitation occurs, and it is easy to distinguish rain-induced attenuation from the overall attenuation A. The RSL under clear-sky conditions is usually assumed to follow a stationary stochastic process, but it changes significantly when it rains. This experiment was conducted in winter when there was less precipitation in the Nanjing area. The number of days in which precipitation occurred was less than one-third of the total number of days, and the days were mainly categorized as light rain days. It is not ideal to use the raw RSL data to generate wet-dry classification. First, the ratio between the RSL data set under sunny conditions and the data set during the precipitation period is not coordinated, which may lead to the classification being biased towards no rain. Second, the experimental data selected in this paper have multiple time-scale disturbances, and the temporal distribution of the RSL contains rich information. The amplitude and attenuation of the RSL are affected by many factors. Therefore, the signal data must be classified more finely.

The information entropy was used to test the degree of abnormality of the signals on each day at the same time scale. The RSL data were divided into the following groups: −40 to −42 dBm, −42 to −44 dBm, −44 to −46 dBm, −46 to −48 dBm, and −48 to −50 dBm. The probability of occurrence of each interval was taken as P_i ($i = 1, 2, 3, 4, 5$). Therefore, the information entropy of the signal data on each day was [12]

$$H = \sum_i -p_i \log(p_i), \quad i = 1, 2, 3, 4, 5. \quad (2)$$

Figure 1: Experimental equipment and the distribution of the MLs.

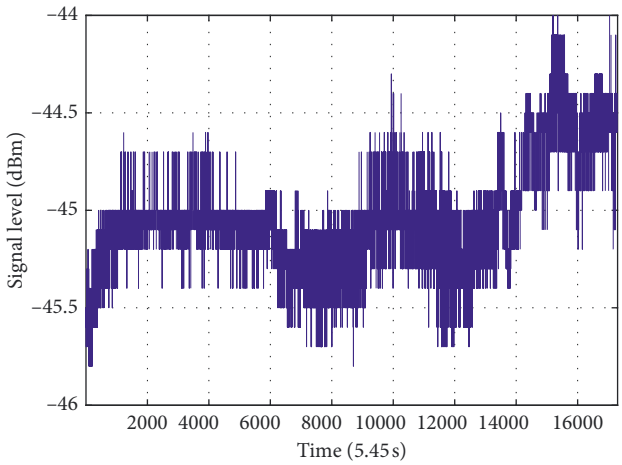

Figure 2: Complex random variation characteristics of the RSL under clear-sky conditions.

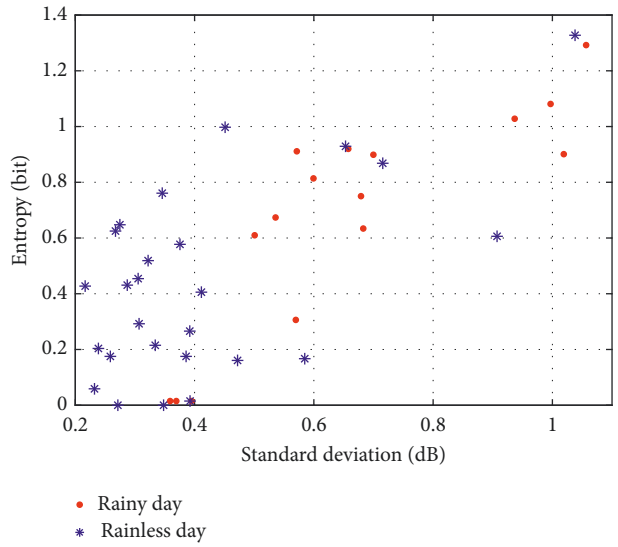

Figure 3: Standard deviation and information entropy distribution of rainy and rainless days from 1st November to 3rd December.

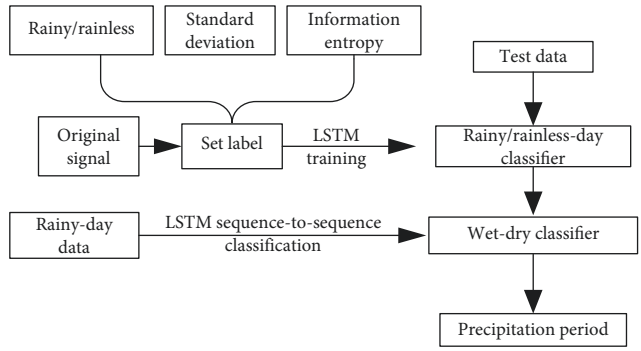

Figure 4: Flow chart of the wet-dry classification.

Taking the RSL for the sampling period of 15 min as an example, Figure 3 shows the information entropy and standard deviation distribution on rainy days (red dots) and rainless days (blue dots) from 1st November to 3rd December. In general, the disturbance of the rainy-day signal is large, and the signal contains more information. However, there are still days when the signal changes abnormally. Signal disturbances on parts of the rainy days are not significant and vary. Some of the rainless-day signals are disturbed, and the change is significant. These anomalous data will cause great interference for the wet-dry classification.

The classification process in this paper is shown in Figure 4. First, we set the labels for each day according to the information entropy, standard deviation, and whether the day was rainy/rainless. Then, we used the trained LSTM network to obtain classifiers that determine whether there is rain on a certain day. Finally, the LSTM sequence-to-sequence classification method was used to train the rainy-day data to obtain classifiers that identify rainfall periods of rainy days.

3.2. LSTM Network Model. Many previously classified algorithms require the data features to have obvious boundary areas in the Euclidean space. However, the data used in this paper, similar to most signal sequences, had continuous variations and unstable random disturbances. It is very difficult to obtain the features from these data that meet the necessary conditions. In this paper, the LSTM algorithm derived from the recurrent neural network (RNN) algorithm, which is sensitive to continuous changes in data, was used as the basic classifier [13]. The construction of such algorithmic neurons relies on the input of the current network layer and contains hidden information from the previous layer. In this way, a temporally sensitive feature of the continuity sequence can be obtained. The LSTM algorithm introduces LSTM modules based on the RNN. When processing the time series, the algorithm is not affected by the time scale of the variation. This has a great advantage when solving the problems of time-series classification.

In this paper, the LSTM model was used to determine the differences in RSL characteristics between precipitation and nonprecipitation periods; these RSLs were classified as dry or wet. x_t indicates the signal feature quantity at time t. The forward-propagating model contains hidden state

units in the RNN h_t. The forward-propagating model includes a hidden state unit in the cyclic neural network, and the learning process is refined by the updated cell state unit C_t. The core formula can be expressed as

$$\begin{aligned} c_t &= c_{t-1} * f_t + i_t * a_t, \\ h_t &= o_t * \tanh(c_t). \end{aligned} \tag{3}$$

The cell state c_{t-1} at time $t-1$ passes through the forget gate f_t at time t, inputs the gate i_t, and updates the cell state c_t at time t. The Hadamard product of the hyperbolic tangent of the output gate o_t of the cell state unit c_t at time t completes the update of the hidden state h_t at time t. The entire forward propagation contains relevant parameters:

$$\begin{aligned} \begin{pmatrix} f_t \\ i_t \\ o_t \end{pmatrix} &= \sigma\left[\begin{pmatrix} W_f \\ W_i \\ W_o \end{pmatrix} x_t + \begin{pmatrix} U_f \\ U_i \\ U_o \end{pmatrix} h_{t-1} + \begin{pmatrix} b_f \\ b_i \\ b_o \end{pmatrix}\right], \\ a_t &= \tanh\left[W_a h_{t-1} + U_a x_t + b_a\right], \end{aligned} \tag{4}$$

where σ is the sigmoid function. We let V be the output weight and then output the predicted value $\hat{y}$ as

$$\hat{y}_t = \sigma(V h_t + c). \tag{5}$$

The weight parameter $W(U)$ and the offset amount b at each moment are determined by backpropagation. The loss function is a cross entropy function [14]:

$$E = \sum_{i=1}^{N} y_i \log(\hat{y}_i) + (1 - y_i)\log(1 - \hat{y}_i). \tag{6}$$

Then, the gradient term for each weight parameter is

$$\begin{aligned} \frac{\partial E}{\partial W_f} &= \sum_{j=1}^{t}\left[\left(\frac{\partial E}{\partial h_j}\right)^{\mathrm{T}} * o_t * \left(1 - \tanh\ (c_t)^2\right) * c_{t-1} * f_t * (1 - f_t)\right] \cdot h_{j-1}, \\ \frac{\partial E}{\partial W_i} &= \sum_{j=1}^{t}\left[\left(\frac{\partial E}{\partial h_j}\right)^{\mathrm{T}} * o_t * \left(1 - \tanh\ (c_t)^2\right) * a_{t-1} * i_t * (1 - i_t)\right] \cdot h_{j-1}, \\ \frac{\partial E}{\partial W_o} &= \sum_{j=1}^{t}\left[\left(\frac{\partial E}{\partial h_j}\right)^{\mathrm{T}} * (1 - \tanh(c_t)) * o_t * (1 - o_t)\right] \cdot h_{j-1}, \\ \frac{\partial E}{\partial W_a} &= \sum_{j=1}^{t}\left[\left(\frac{\partial E}{\partial h_j}\right)^{T} * o_t * \left(1 - \tanh\ (c_t)^2\right) * i_t * \left(1 - a_t^2\right)\right] \cdot h_{j-1}, \\ \frac{\partial E}{\partial U_f} &= \left[\left(\frac{\partial E}{\partial h_t}\right)^{\mathrm{T}} * o_t * \left(1 - \tanh\ (c_t)^2\right) * c_{t-1} * f_t * (1 - f_t)\right] \cdot x_t, \\ \frac{\partial E}{\partial U_i} &= \left[\left(\frac{\partial E}{\partial h_t}\right)^{\mathrm{T}} * o_t * \left(1 - \tanh\ (c_t)^2\right) * a_t * i_t * (1 - i_t)\right] \cdot x_t, \\ \frac{\partial E}{\partial U_o} &= \left[\left(\frac{\partial E}{\partial h_t}\right)^{\mathrm{T}} * \tanh(c_t) * o_t * (1 - o_t)\right] \cdot x_t, \\ \frac{\partial E}{\partial U_a} &= \left[\left(\frac{\partial E}{\partial h_t}\right)^{\mathrm{T}} * o_t * \left(1 - \tanh\ (c_t)^2\right) * i_t * \left(1 - a_t^2\right)\right] \cdot x_t. \end{aligned} \tag{7}$$

The gradient term for each offset is

$$\begin{aligned} \frac{\partial E}{\partial b_f} &= \sum_{j=1}^{t}\left(\frac{\partial E}{\partial h_j}\right)^{\mathrm{T}} * o_t * \left(1 - \tanh\ (c_t)^2\right) * c_{t-1} * f_t * (1 - f_t), \\ \frac{\partial E}{\partial b_i} &= \sum_{j=1}^{t}\left(\frac{\partial E}{\partial h_j}\right)^{\mathrm{T}} * o_t * \left(1 - \tanh\ (c_t)^2\right) * a_{t-1} * i_t * (1 - i_t), \\ \frac{\partial E}{\partial b_o} &= \sum_{j=1}^{t}\left(\frac{\partial E}{\partial h_j}\right)^{\mathrm{T}} * (1 - \tanh(c_t)) * o_t * (1 - o_t), \\ \frac{\partial E}{\partial b_a} &= \sum_{j=1}^{t}\left(\frac{\partial E}{\partial h_j}\right)^{\mathrm{T}} * o_t * \left(1 - \tanh\ (c_t)^2\right) * i_t * \left(1 - a_t^2\right). \end{aligned} \tag{8}$$

4. Classification Results

4.1. Rainy-Day/Rainless-Day Classification Effects. This section uses the data from 1st November to 30th November to train a classifier that distinguishes between rainy and rainless days. The December data were used as test data to evaluate the classifier's results. To analyze the overall change in each day's signal, we set the sampling period to 15 min. A total of 96 continuous RSL samples were obtained per day. To retain more information about the signal, a standard deviation of 15 min was used as the second set of training data, and the 30-day data were divided into 30 sets of data with a step size of 24 h. In this section, 30 sets of data were given four label types: 1 means no rain and normal data, 2 means no rain and abnormal data, 3 means rain and abnormal data, and 4 means rain and normal data. We determined whether each signal was normal using information entropy and standard deviations. For rainy days, the days when the information entropy was ≥0.6 and the standard deviation was ≥0.5 indicated that the signal was normal, and the opposite occurred for abnormal rainy days. For rainless days, the days when the information entropy was >0.6 or the standard deviation was >0.5 indicated that the signal was abnormal, and the opposite occurred for normal rainless days. The labels are shown in Table 1.

The ideal RSL is a superposition of a stable signal level and randomly distributed stationary noise. The mean value of the RSL is always at a certain level. However, when analyzing the time-varying characteristics of the RSL under clear-sky conditions, the mean value of the RSL shows a significant change (Figure 2). In addition to rain, there are other factors that cause changes in the RSL. Therefore, the RSL changes caused by precipitation need to be distinguished by the relative variation characteristics of the RSL. The data from the training set were normalized to obtain the relative change in the RSL within one day. When the length of the input data x is n, x is normalized as

$$x_i = \frac{x_i - (1/n)\sum_{i=1}^{n} x_i}{(1/n)\sum_{i=1}^{n}\sqrt{\left(x_i - (1/n)\sum_{j=1}^{n} x_j\right)^2}}. \tag{9}$$

Table 1: Classification labels for 30-day test data.

Label	Information entropy (bit)	Standard deviation (dB)	Number of days	Rainy/no rain
1	≤0.6	≤0.5	13	No rain
2	Information entropy >0.6 or standard deviation >0.5		7	No rain
3	Information entropy <0.6 or standard deviation <0.5		4	Rainy
4	≥0.6	≥0.5	6	Rainy

The other set of inputs includes the standard deviation of the signal every 15 min. This was used as a measure of the relative mean disturbance over 15 min periods, and it was not normalized. Thirty sets of two-dimensional data and their corresponding labels from 30 days were input into the LSTM network for training to obtain rainy/rainless-day classifiers. The data were trained 500 times with an accuracy rate of 100%. The accuracy and loss curves of the training data are shown in Figure 5.

Twenty-two days of data in December were substituted into the rainy-day/rainless-day classifier generated by the LSTM network. The classification effect is shown in Figure 6. The dark areas in the picture indicate rainy days. Labels 3 and 4 in the classification indicate rainy days. The classifier identified a total of 9 days with the label 4 and 1 day with the label 3. In reality, precipitation occurred on these ten days. In total, there were 11 real rain-free days, and the predicted result was 0 or 1. Only the rainy day on 26th December was incorrectly identified as label 2, and the classified results of the other 21 rainy/rainless days were correct. According to the data from the rain gauge on 26th December, there was light rain almost all day. The classifier judged it as label 2 (no rain and abnormal data), which may be because the occurrence of rain almost all day caused the signal to exhibit a specific characteristic almost the entire time, so the difference in signal change under the two different conditions of rainy/rainless was not obvious. Although it did not accurately judge whether it was rainy, the classifier accurately determined that the signal that day contained a large amount of information. In practical applications, the days marked as 2 by the classifier need special attention. Under normal conditions, for days with rain all day, the RSL on that day should show significant attenuation compared to the signal attenuation on the two days before and after that day. By comparing the attenuation difference, it may be possible to avoid missing rainy days.

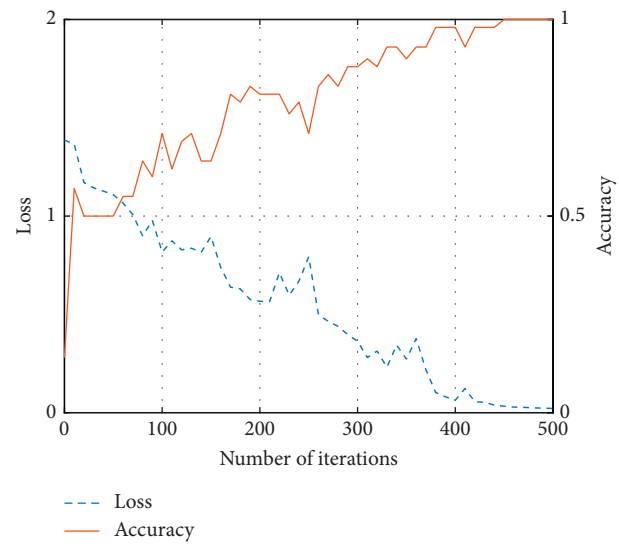

Figure 5: Loss and accuracy curves of rainy-day/rainless-day classifier training.

4.2. Classification Results of Wet-Dry Periods of Rainy Days. Rainy days can be identified by the classifier set up in the previous section. Next, the wet-dry classifiers for rainy days were set up on the premise of identifying rainy days, where rainy-day data were used. A time-series classifier that outputs precipitation information through a series of signals requires an increased time resolution. This study mainly used the tipping bucket rainfall method to determine the precipitation period; however, the rain gauge had a limited rain rate resolution. The resolution of the tipping bucket rain gauge is limited to 6 mm/h as the instrument just records the number of tips every minute, with no information on when in that minute a specific tip occurred. Although the tipping bucket rain gauge can accurately record the cumulative precipitation, there is a limitation to identify the exact time that light rain occurred. Considering that the rain gauge is located at the receiving terminal, no rain measured by the rain gauge does not mean that the entire 19.74 km path is rain free, especially in the case of an extremely uneven spatial distribution of precipitation, and the time resolution of the signal data does not match the time resolution of the rain gauge data. To solve such problems, we set a certain length for the time window w. The rain gauge data R in the time window were averaged, and the length of the original rain gauge data was L:

$$R_w(t) = \begin{cases} 1, & \text{if } \max(R[t+1, t+w]) > 0, \\ 0, & \text{if } \max(R[t+1, t+w]) = 0, \end{cases} \quad t = 0, w, 2w, \ldots, L-w, \tag{10}$$

where max represents the maximum function, $R[t+1, t+w]$ indicates the rain gauge data from $t+1$ to $t+w$, and R_w is the label of the input signal data. Eleven data signals were recorded per minute. The maximum RSL in the time window $11 \times w$ was selected. The precipitation that occurred during the experiment was dominated by light rain. When w was less than 5, periods with rain rates less than 1 mm/h could not be identified. Therefore, this study used 5, 10, and 15 min time windows for the analysis.

To judge the stability of the algorithm for constructing the wet-dry classifier, first, the November rainy-day RSLs and rainfall data were used as the training set to obtain the LSTM wet-dry classifiers with three time resolutions (5, 10, and 15 min). The December RSLs were used as test data to obtain the accuracies of the three classifiers on each day, where the results are shown in Figure 7(a). Then, the

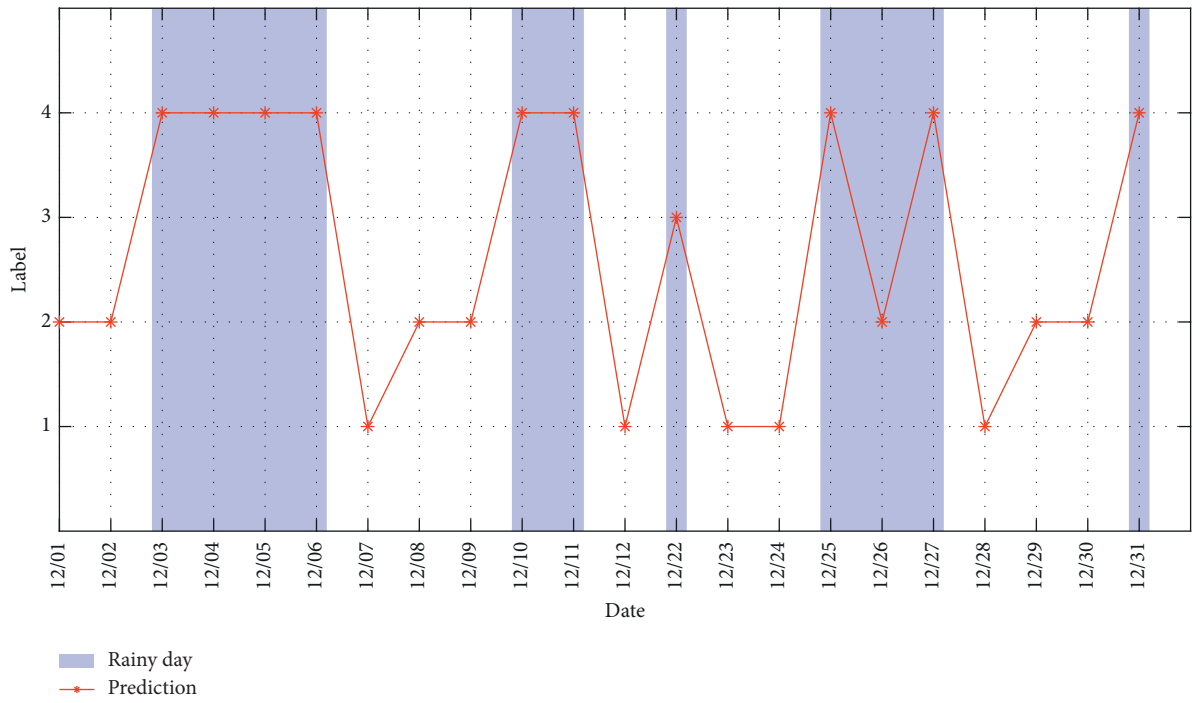

Figure 6: Classification effect of the rainy-day/rainless-day classifier.

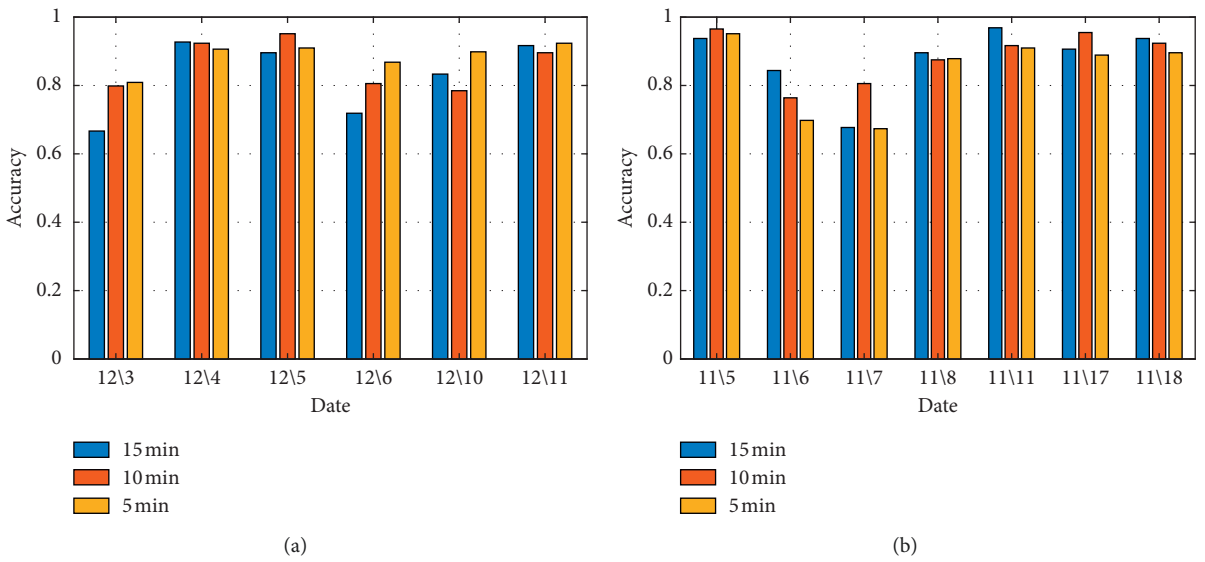

Figure 7: Accuracy of each day's classification determined by the wet-dry classifiers at three resolutions constructed by two sets of training data. (a) December. (b) November.

December data were used as the training set, and the classifiers were obtained at the three time resolutions. The wet-dry classification accuracy of the signal data in November was obtained, as shown in Figure 7(b).

From an accuracy perspective, the classification effect of the classifier was shown to be ideal. Regardless of the resolution, the accuracy each day was higher than 60%, and the accuracies on some days were even higher than 98%. In terms of numerical values, different classifiers showed different effects for different rainy days. The temporal characteristics of the signal were different on each day, so the responses of each signal to the classifier at each resolution were also different. Overall, excluding 11th November, the classifier with a time resolution of 15 min had no significant advantage, and the other days with higher accuracy levels always showed similar results in the other two classifiers. To visually analyze the effects of the three classifiers, a representative day was selected to discuss the time distributions of the RSL, the labels of the rain gauge, and the classified results (Figure 8).

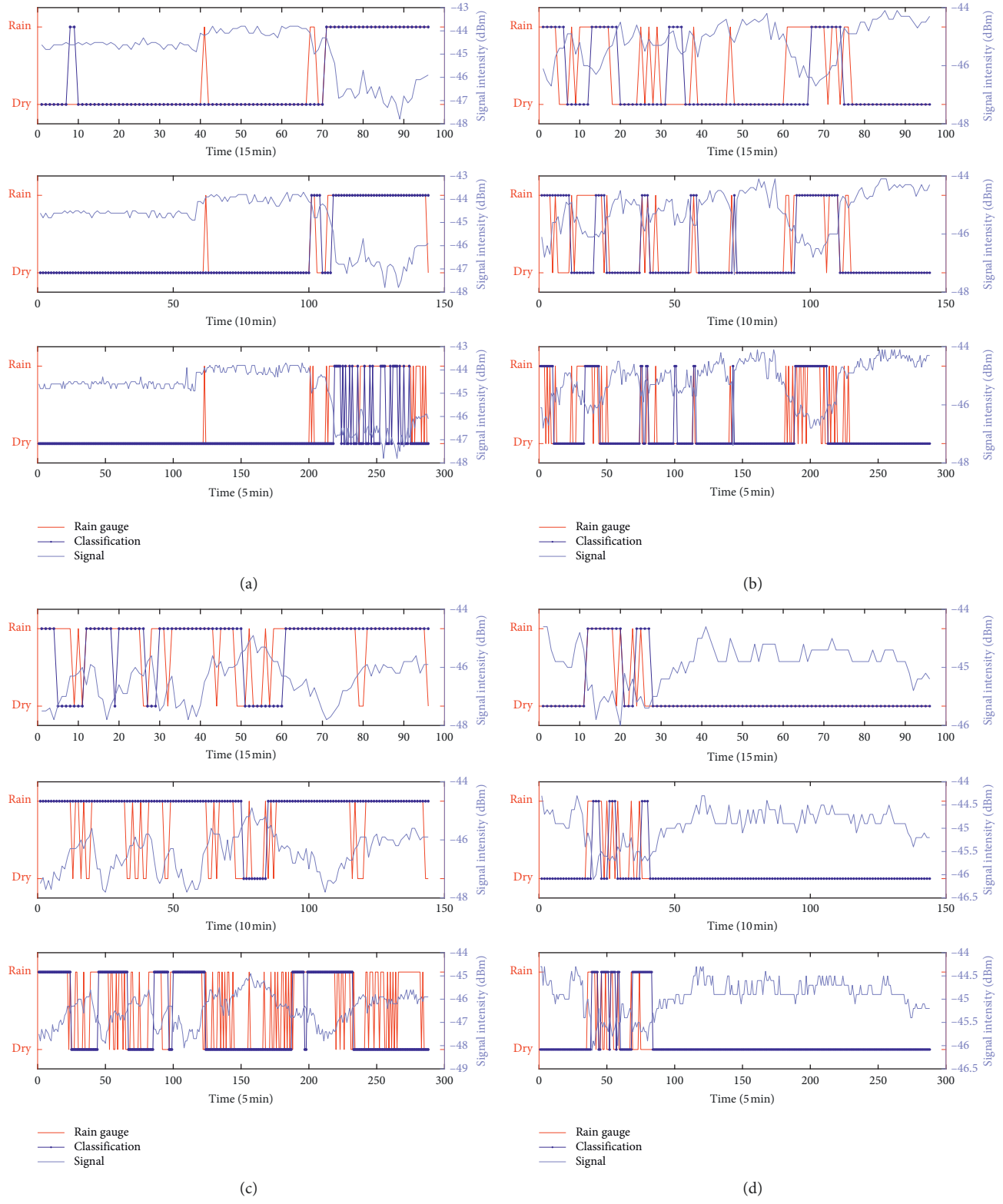

Figure 8: Results of the wet and dry periods. (a) 5th December. (b) 6th December. (c) 7th November. (d) 11th November.

Figures 8(a) and 8(b) show the classification results of the wet and dry periods on 5th and 6th December using the classifier constructed with the November data. The red line denotes R_w (Rain gauge), the blue dotted line denotes the classification results (Classification), and the light-colored line denotes the original RSL of the input classifier (RSL). For the 15 min time window, the classification of long-term and continuous precipitation is not ideal. The precipitation

results during long periods are not detailed enough, and the effect is obviously not as good as that during the other two time windows. Comparing the two time windows of 10 and 5 min, the latter classifier has a tendency to identify the occurrence of precipitation in the absence of rain mistakenly. Although the classification accuracy rate is higher for the 5 min time window, the classifier with the 10 min time window can identify light rain attenuation and is not easily influenced by nonprecipitation factors in the dry period, which may be because of the limitations of the rain gauge. This classifier has no data under the condition that the average rain rate during one minute is less than 6 mm/h. Meanwhile, although there was no rain around the terminal's rain gauge, the 19.74 km path may have an uneven precipitation spatial distribution, especially for convective rainfall.

Figures 8(c) and 8(d) show the results of the wet and dry period classification on 7th and 11th November using the classifier constructed with the December data. The classification results on 7th November are representative of most experimental data, and the classification effect on most days is similar. The resolution of the 15 min classifier is too low, and the 5 min classifier easily misjudges wet periods as dry periods. For intermittent precipitation, the 10 min time window classifier is clearly more realistic. Limited by the rain gauge resolution, extremely short intermittent dry periods classified by the rain gauge are very likely to be wet periods. The classifier with the 10 min time window not only distinguishes continuous precipitation periods but also does not miss obvious dry periods. Data from 11th November represent a special case. In the case where the all-day rainfall is concentrated within one time period and the duration is short, the 15 min classifier has a relatively low resolution, but the classified result is not only higher in terms of accuracy but also more realistic. Short-term precipitation is more common with convective rainfall. In this case, the rainfall time period is short and concentrated, and the classifier also has the ability to distinguish dry periods between two concentrated short-term periods of precipitation.

In practical applications, when precipitation data are limited by the space-time resolution, the scale of the time window should be appropriately controlled. Convective precipitations are much more uneven in space and time, which reduces the accuracy of the classification algorithm. However, if the time window is too long, the resolution of the algorithm is constrained. Therefore, the choice of the length of the time window is especially important for the classification algorithm described in this paper. The selection of the time window scale is affected by the frequency of the ML, the type of rainfall (convective rainfall or stratiform rainfall), the length of the ML, and the accuracies of the rain gauges. Under such circumstances, in practical operations, the results under multiple time windows should be compared. When the time distribution of rainfall is more concentrated, it seems that the classifier set up with a long time window is more reliable. For intermittent rainfall, it is more reasonable to use a shorter time window. To improve the temporal resolution of the algorithm, reliable and accurate rainfall data in the path are essential.

It is worth noting that we conducted experiments in the winter season when rainfall was light in Nanjing. The spatial and temporal distributions of rainfall may vary significantly in different seasons. For example, when there is heavy rain in summer, the rain-induced attenuation in the MLs would be substantial, and the temporal distribution of rainfall in the Meiyu rainy season would be significantly different. The RSLs of the MLs under the above conditions may have more complicated distributions. Therefore, it is necessary to add data from different seasons to train the model, and different seasons may even be needed to construct different classifiers to improve the classified effect.

5. Conclusions

This study applied the C-band ML signal to construct two LSTM network classifiers. The RSLs were processed step by step to classify the dry and wet periods in the low-frequency band with noisy and unstable MLs. Additionally, a classification strategy for the signals of wet and dry periods with large disturbances and light rain attenuation was proposed. Finally, the influences of sampling periods with different time scales on the classification results were analyzed. Regardless of the time window scale, the accuracy of classification on each day was higher than 60%, and the accuracies on some days were even higher than 98%. The following conclusions were drawn from this study:

(1) MLs below 10 GHz have the potential to monitor ground rainfall. Although their resolutions are limited in areas with complex terrain and uneven climate condition distributions, under light rain conditions, it is possible to determine whether precipitation occurs within the ML. These MLs also have some reference significance for the analysis of precipitation in two-dimensional areas. The results of this study increase the amount of applicable equipment available for measuring precipitation via MLs.

(2) This study analyzed the method for distinguishing between wet and dry periods with larger disturbances and irregular signals and determined certain reference significance for baseline estimation problems, such as baseline drift and precipitation inversion. Unstable signals within a certain degree of disturbance can also reflect precipitation information, further highlighting the potential to use MLs to measure precipitation.

(3) This study divided the wet-dry classification into two steps: In the first step, although rainy-day identification for all-day precipitation is limited, overall, most types of rainy days can be identified. In the second step of the wet-dry classification, the accuracy is higher than 80% when selecting the appropriate time window. For short-term precipitation, increasing the scale of the time window appropriately can improve the classification results.

In the future, we will conduct experiments in different seasons to ensure the universality of the algorithm and

perform further research on calculating the rain rate via C-band MLs on the basis of wet-dry classification.

Data Availability

The data used to support the findings of this study are available from the corresponding author upon request.

Conflicts of Interest

The authors declare no conflicts of interest.

Acknowledgments

This research was supported by the National Natural Science Foundation of China (Grant nos. 41505135 and 41475020).

References

[1] H. Messer, A. Zinevich, and P. Alpert, "Environmental monitoring by wireless communication networks," *Science*, vol. 312, no. 5774, p. 713, 2006.

[2] D. Noam, A. Pinhas, and M. Hagit, *Flash Floods Warning Technique Based on Wireless Communication Networks Data*, Real Time, Chicago, IL, USA, 2010.

[3] J. Ostrometzky, R. Raich, A. Eshel, and H. Messer, "Calibration of the attenuation-rain rate power-law parameters using measurements from commercial microwave networks," in *Proceedings of the 2016 IEEE International Conference on Acoustics, Speech and Signal Processing (ICASSP)*, pp. 3736–3740, Shanghai, China, March 2016.

[4] A. Overeem, H. Leijnse, and R. Uijlenhoet, "Measuring urban rainfall using microwave links from commercial cellular communication networks," *Water Resources Research*, vol. 47, no. 12, 2011.

[5] T. C. van Leth, A. Overeem, H. Leijnse, and R. Uijlenhoet, "A measurement campaign to assess sources of error in microwave link rainfall estimation," *Atmospheric Measurement Techniques*, vol. 11, no. 8, pp. 4645–4669, 2018.

[6] M. Schleiss and A. Berne, "Identification of dry and rainy periods using telecommunication microwave links," *IEEE Geoscience and Remote Sensing Letters*, vol. 7, no. 3, pp. 611–615, 2010.

[7] Z. Wang, M. Schleiss, J. Jaffrain, A. Berne, and J. Rieckermann, "Using Markov switching models to infer dry and rainy periods from telecommunication microwave link signals," *Atmospheric Measurement Techniques Discussions*, vol. 5, no. 1, pp. 411–445, 2012.

[8] H. Leijnse, R. Uijlenhoet, and J. N. M. Stricker, "Hydrometeorological application of a microwave link: 2. Precipitation," *Water Resources Research*, vol. 43, no. 4, pp. 244–247, 2007.

[9] O. Goldshtein, H. Messer, and A. Zinevich, "Rain rate estimation using measurements from commercial telecommunications links," *IEEE Transactions on Signal Processing*, vol. 57, no. 4, pp. 1616–1625, 2009.

[10] C. S. Ruf, K. Aydin, S. Mathur, and J. P. Bobak, "35-ghz dual-polarization propagation link for rain-rate estimation," *Journal of Atmospheric & Oceanic Technology*, vol. 13, no. 2, pp. 419–425, 1996.

[11] O. Harel and H. Messer, "Extension of the MFLRT to detect an unknown deterministic signal using multiple sensors, applied for precipitation detection," *IEEE Signal Processing Letters*, vol. 20, no. 10, pp. 945–948, 2013.

[12] J. A. Núñez, P. M. Cincotta, and F. C. Wachlin, "Information entropy," in *Chaos in Gravitational N-Body Systems*, vol. 64, pp. 43–53, no. 1-2, Springer, Dordrecht, Netherlands, 1996.

[13] S. Hochreiter and J. Schmidhuber, "Long short-term memory," *Neural Computation*, vol. 9, no. 8, pp. 1735–1780, 1997.

[14] P. Vincent, H. Larochelle, I. Lajoie, Y. Bengio, and P. A. Manzagol, "Stacked denoising autoencoders: learning useful representations in a deep network with a local denoising criterion," *Journal of Machine Learning Research*, vol. 11, no. 12, pp. 3371–3408, 2010.